Cerebral Cortex, January 2019;29: 1–16

doi: 10.1093/cercor/bhx291
Advance Access Publication Date: 9 November 2017
Original Article

ORIGINAL ARTICLE

The Laminar Organization of Piriform Cortex Follows a Selective Developmental and Migratory Program Established by Cell Lineage

Eduardo Martin-Lopez[1], Kimiko Ishiguro[1] and Charles A. Greer[1,2,3]

[1]Department of Neurosurgery, Yale University School of Medicine, 333 Cedar Street, New Haven, CT 06520, USA, [2]Department of Neuroscience, Yale University School of Medicine, 333 Cedar Street, New Haven, CT 06520, USA and [3]The Interdepartmental Neuroscience Graduate Program, Yale University School of Medicine, 333 Cedar Street, New Haven, CT 06520, USA

Address correspondence to Dr Charles A. Greer. Email: charles.greer@yale.edu

Abstract

Piriform cortex (PC) is a 3-layer paleocortex receiving primary afferent input from the olfactory bulb. The past decade has seen significant progress in understanding the synaptic, cellular and functional organization of PC, but PC embryogenesis continues to be enigmatic. Here, using birthdating strategies and clonal analyses, we probed the early development and laminar specificity of neurogenesis/gliogenesis as it relates to the organization of the PC. Our data demonstrate a temporal sequence of laminar-specific neurogenesis following the canonical "inside-out" pattern, with the notable exception of PC Layer II which exhibited an inverse "outside-in" temporal neurogenic pattern. Of interest, we found no evidence of a neurogenic gradient along the anterior to posterior axis, although the timing of neuronal migration and laminar development was delayed rostrally by approximately 24 h. To begin probing if lineage affected cell fate in the PC, we labeled PC neuroblasts using a multicolor technique and analyzed their laminar organization. Our results suggested that PC progenitors were phenotypically committed to reach specific layers early in the development. Collectively, these studies shed new light on the determinants of the laminar specificity of neuronal/glial organization in PC and the likely role of subpopulations of committed progenitors in regulating PC embryogenesis.

Key words: cell clones, piggyBac, projection neurons, birthdating analysis, layering

Introduction

The piriform cortex (PC), which contributes to odor coding and representation, receives primary afferent odor information via monosynaptic input from the olfactory bulb (OB) projection neurons, mitral and tufted cells. In rodents, the PC occupies the most ventrolateral aspect of the brain and includes ~1 000 000 neurons (Srinivasan and Stevens 2017). The PC is flanked dorsolaterally by the rhinal fissure and ventrally by the olfactory tubercle. Rostrally it continues as the anterior olfactory nucleus (AON) and caudally it merges with the entorhinal cortex.

The PC is divided into 3 layers, a characteristic feature of paleocortical or allocortical structures, whose primary cytoarchitecture was characterized more than a century ago (Calleja 1893; Ramon y Cajal 1901; O'Leary 1937). The outermost layer of PC is the lateral olfactory tract (LOT) formed by the axon fascicles that include afferent input from the OB. Layer Ia is immediately deep to the LOT and is primarily neuropil with axodendritic synapses from the LOT axons. Layer Ib is also primarily neuropil, including axodendritic synapses from cortico-cortico association axons and few populations of interneurons morphologically classified as

horizontal, globular neurogliaform and multipolar cells (Haberly et al. 1987; Suzuki and Bekkers 2007). Layer II is well defined with the somata of superficial pyramidal and semilunar neurons forming a compact band of projection neurons. Finally, Layer III includes sparse deep pyramidal neurons. Local inhibitory neurons are scattered throughout all 3 layers. Synaptic interactions occur predominately within the neuropil of Layer I, which may reflect its involvement in epileptogenesis (Uva et al. 2017).

The representation of odors in PC was initially believed to be sparsely distributed throughout PC (Haberly 2001; Nagayama et al. 2010), in which small ensembles of PC neurons exhibited distinguishable odor identities (Poo and Isaacson 2009; Stettler and Axel 2009; Bekkers and Suzuki 2013). More recent reports suggest the response of PC neurons may not be sparse (Davison and Ehlers 2011; Bolding and Franks 2017), involving a more complex distribution of odor representation in PC (Choy et al. 2017; Roland et al. 2017; Tantirigama et al. 2017; Yang et al. 2017).

Despite the significant efforts devoted to understanding the physiology of PC, less attention has been paid to the cellular and molecular events that occur during the development of PC, and paleocortex more generally. PC cells derive mainly from the lateral ganglionic eminence (LGE), with secondary contributions from the rostral telencephalon and ventral pallium (Garcia-Moreno et al. 2008; Ceci et al. 2012; Pedraza and De Carlos 2012) following ventral and caudal migratory routes (Carney et al. 2006; Huilgol and Tole 2016). These cells express transcription factors similarly to the neocortex and mature differentially depending on the embryonic day of generation (Sarma et al. 2011; Brunjes and Osterberg 2015). However, we continue to lag in our understanding of the processes of embryogenesis and lamination in PC and the potential for differences in organization along the posterior–anterior axis. Moreover, the degree to which common or shared progenitors may be important in establishing PC cellular fate is largely unknown.

Using classical birthdating analyses we show for the first time an extensive neurogenic map for PC cells along the anterior–posterior axis throughout the layers and sublayers of PC. Also, we report a detailed analysis of the migratory behavior of PC precursor cells from the LGE to their final destinations in the PC while describing their morphometric and phenotypic characteristics. Finally, we used innovative strategies based on the expression of different combinations of fluorescent proteins (Livet et al. 2007; Weber et al. 2011; Garcia-Marques and Lopez-Mascaraque 2013; Martin-Lopez et al. 2013; Garcia-Moreno et al. 2014; Xiong et al. 2015), to study PC cell phenotypes and investigate the possibility of cell lineages that shared a common progenitor. Specifically, we applied a multicolor labeling technique similar to the UbC-StarTrack method (Figueres-Onate et al. 2016) to test that clonal relationships are likely an important determinant of PC cellular fate.

Materials and Methods

Animals

All experiments were conducted on litters from pregnant CD1 mice and included both males and females. All animals were obtained from Charles River Laboratories and housed on a 12-h light cycle with access to standard chow ad libitum. All procedures were approved by Yale University Animal Care and Use Committee.

Injection of Thymidine Analogs and Processing of Tissue

The neurogenesis and gliogenesis of PC was studied by injections of thymidine analogs in mice (Wojtowicz and Kee 2006; Zhao et al. 2007). Pregnant females at the embryonic ages (E) of E10, 11, 12, 13, 14, 15, 16, 17 ($n = 3$), and E18 ($n = 2$) were given a single I.P injection of 50 mg/kg of BrdU (BD Biosciences) between 10–11 am. Additional groups of mice received I.P. 50 mg/kg injections of both thymidine analogs IdU and CldU (Sigma-Aldrich), but separated by 48 h. These injections occurred at either E11 and E13 ($n = 3$) or at E12 and E14 ($n = 3$). The offspring of the IdU/CldU injected animas were analyzed at the postnatal (P) ages of P0, P7, P14, and P21, while BrdU injected animals were studied exclusively at P21. Pups were euthanized with an overdose of Euthasol (Virbac) and transcardially perfused with 4% paraformaldehyde (PFA, JT Baker) in phosphate buffered saline (PBS). Then brains were dissected from skulls, postfixed overnight in 4%-PFA/PBS, and cryoprotected in 30% Sucrose-PBS (Aldon Corporation SE) at 4 °C before sectioning. Brains were embedded in OCT-compound (Fisher Scientific) and 30 µm coronal sections were collected serially using a Reichert Frigocut Cryostat (E-2800). Tissue sections were air dried and kept at −80°C until processing for immunohistochemistry.

Nissl Staining

A P21 set of tissue sections were rehydrated and stained by incubating them in a 0.1% toluidine blue dye (Sigma-Aldrich) solution for 1 min. The excess of colorant was washed out with running water and the colorant was differentiated in 95% ethanol. Finally, the sections were dehydrated in 100% ethanol and xylene and mounted with DPX mounting medium (Fluka).

Immunostaining

Sections were thawed at 60 °C on a slide warmer and subsequently treated for antigen retrieval by changing slides 3 times from boiling to ice-cooled 0.01 M citrate buffer pH6.0. Exclusively for those sections containing thymidine analogs, the DNA was denatured using a 0.02 M HCl solution incubated at 65°C for 35 min. Non-specific antibody binding was blocked by incubating sections with a solution of PBS containing 0.1% Triton × 100 (Sigma-Aldrich) (PBST) supplemented with 5% Normal Goat Serum (NGS, Accurate Chemicals) + 0.1% Bovine Serum Albumin (BSA, Sigma-Aldrich) for 1 h at room temperature. Then, primary antibodies diluted in blocking solution (Table 1) were added to slides and incubated overnight at 4°C. Sections were rinsed 3 times with PBST and incubated for 2 h at room temperature with a solution of PBST containing specific secondary antibodies (Table 1), 1 µg/mL of DAPI (Invitrogen) and 5 µM DRAQ5 (BD Pharmingen) for nuclear counterstaining. Sections were washed with PBST and mounted with Mowiol (Sigma-Aldrich).

Expression Plasmids for Multicolor Labeling

Cell lineages were assessed using a multicolor technique based on the stochastic expression of 3 spectrally different fluorophores introduced from piggyBac plasmids into genomic DNA of progenitor cells (Supplementary Fig. 1A). This system was previously used effectively to track cell lineages (Livet et al. 2007; Weber et al. 2011; Garcia-Marques and Lopez-Mascaraque

Table 1. Primary and secondary antibodies

Antigen	Primary AB	Source (ref)	Dilution	Secondary Ab	Source	Dilution
BrdU (CldU)	Rat IgG	Accurate Chem. (OBT0030)	1:300	Goat anti-rat IgG Alexa 488	Invitrogen	1:1000
BrdU (IdU)	Mouse IgG	BD Biosciences (347580)	1:200	Goat anti-ms IgG Alexa 546	Invitrogen	1:1000
Calretenin	Mouse IgG1	EMD Millipore (MAB1568)	1:400	Goat anti-ms IgG1 Alexa 546	Invitrogen	1:1000
Doublecortin	Rabbit Poly.	Cell Signaling (4604)	1:500	Goat anti-rbt IgG Alexa 546	Invitrogen	1:1000
GABA	Rabbit IgG	Sigma-Aldrich (A2052)	1:300	Goat anti-rbt IgG Alexa 546	Invitrogen	1:1000
GAD65/67	Mouse IgG2a	EMD Millipore (MAB5406)	1:200	Goat anti-ms IgG2a Alexa 546	Invitrogen	1:1000
GFAP	Rabbit Poly.	Dako (Z0334)	1:500	Goat anti-rbt IgG Alexa 546	Invitrogen	1:1000
Iba1	Rabbit IgG	Wako (016-2000001)	1:200	Goat anti-rbt IgG Alexa 546	Invitrogen	1:1000
Map2	Chicken IgG	EMD Millipore (AB5543)	1:500	Goat anti-Chicken Alexa 568	Invitrogen	1:1000
NeuN	Mouse IgG1	EMD Millipore (MAB377)	1:500	Goat anti-ms IgG1 Alexa 546	Invitrogen	1:1000
Parvalbumin	Rabbit IgG	Abcam (ab11427)	1:100	Goat anti-rbt IgG Alexa 546	Invitrogen	1:1000
PSA-NCAM	Mouse IgM	EMD Millipore (MAB5324)	1:250	Goat anti-ms IgM Alexa 555	Invitrogen	1:1000
Reelin	Mouse IgG	EMD Millipore (ab78540)	1:500	Goat anti-ms IgG Alexa 546	Invitrogen	1:1000
S100β	Mouse IgG1	Sigma-Aldrich (S2532)	1:100	Goat anti-ms IgG1 Alexa 546	Invitrogen	1:1000
Tbr1	Rabbit Poly.	EMD Millipore (ab31940)	1:500	Goat anti-rbt IgG Alexa 546	Invitrogen	1:1000

2013; Martin-Lopez et al. 2013; Xiong et al. 2015). Here, we are using a modification of the technique previously introduced as the UbC-StarTrack method (Figueres-Onate et al. 2016). The donor plasmids we used included 3 different piggyBac transposons expressing the following fluorophores: (1) an EGFP piggyBac transposon (pPB-CAG-EGFP) (kindly donated by Andrew K. Groves, Baylor College of Medicine); (2) a tdTomato piggyBac transposon (pPB-CAG-tdTomato), prepared by cloning the tdTomato sequence from pCAG-tdTomato (kindly donated by Angelique Bordey, Yale University) into the previous plasmid; (3) a plasmid expressing a far-red emitting fluorophore (pPB-CAG-iRFP670), prepared by cloning the iRFP670 sequence from piRFP670-N1 (Addgene plasmid #45457) (Shcherbakova and Verkhusha 2013) into pPB-CAG-EGFP. The helper plasmid was a vector expressing the transposase enzyme under the CAG promoter (pCAG-PBase, kindly donated by Andrew K. Groves).

Plasmids were amplified in transformed bacteria and DNAs purified using an Endo-free plasmid MaxiPrep kit according to the manufacturer's protocol (QIAGEN). DNAs pellets were resuspended in sterile water and kept at −20°C until use. Prior to injection, a mixture of the donor plasmids (all 3 for cell lineage analyses at 0.7 μg/mL, or just one to combine cell labeling with immunostaining at 1 μg/mL) with the helper plasmid at 1 μg/mL was prepared in water containing 0.05% fast green (Sigma-Aldrich).

Validation of Plasmids on HEK Cell Cultures

The absence of excitation/emission spectra overlapping from the 3 different fluorophores cloned into piggyBac plasmids was tested in vitro on HEK cells (Supplementary Fig. 2). Briefly, HEK human embryonic kidney 293 T cells, (obtained from Peter Tattersall, Yale University) were maintained in DMEM/F12 medium supplemented with 10% FBS (Gibco) and 50 units/mL of penicillin and 50 μg/mL of streptomycin. STR profiling conducted by Yale DNA Analysis Facility showed that the cells were an 86% percent match to the ATCC human cell line CRL-3216 [HEK 293 T]. For transfection, cells were plated at a density of 3×10^4 cells/well in 0.3 mL medium in Falcon 8 Chamber Tissue Culture Treated Glass Slide (Corning). At Day 1, 0.5 μg of DNA from each donor plasmid and 1 μL of Lipofectamine 2000 (Invitrogen) were premixed in 40 μl of Opti-MEM (Invitrogen) and added to cultured cells. At Day 2, cells were fixed with ice-cold 4% paraformaldehyde in PBS for 10 min. After the chambers were removed, the glass slides were mounted with Mowiol and subjected to fluorescence analysis.

In Utero Injection and Electroporation

PC lineages were studied by inserting fluorescent markers into progenitor cells located in the LGE, an area that can be targeted by in utero electroporation (Pedraza and De Carlos 2012). Electroporations were made at E11 to induce a stochastic expression of 1, 2, or 3 fluorophores creating unique and inheritable marker in each progenitor cell giving rise to both neurons and glial cells (Supplementary Fig. 1C).

Minutes before surgery, the mixture of plasmids was loaded in a borosilicate capillary previously pulled to obtain a thin tip of ~50 μm diameter. Pregnant females were deeply anesthetized with a solution of 100 mg/kg Ketamine (Ketaset, Pfizer) + 10 mg/kg Xylazine (AnaSed, Lloyd) and placed on their back on a microwavable heating pad. An incision was made in the midline of the abdominal skin and the peritoneal membrane was cut through the alba line. Both uterine horns were pulled out from the abdominal cavity and kept warm and hydrated by delivering prewarmed sterile saline solution (Hospira). One of the cerebral lateral ventricles of each embryo was filled with approximately 0.2–0.5 μL of the plasmid(s) solution, injected with a Picospritzer (Parker) using 5–10 pulses of 10 psi of pressure and 5 ms duration per pulse. Embryos were gently hydrated with saline solution and an electrical current was applied using a pair of gold tweezers (Genepaddles-542, Harvard Apparatus) connected to an ECM 830 electroporator (BTX Harvard Apparatus). The electrodes were placed in an orientation so that the cathode was aligned with the ventrolateral axis of the embryo head where the future PC will develop to target the LGE (Supplementary Fig. 1B). Electroporation was achieved by delivering 5 pulses of 35 V (5 ms duration at intervals of 950 ms) to each embryo. Uterine horns were rapidly rehydrated and introduced back into the abdominal cavity. The peritoneal membrane was closed using a 5/0 PGA absorbable suture (AD Surgical) and the skin was sutured using a 5/0 silk braided suture (Ethicon). The wound was cleaned and a protective scar antibiotic ointment (Neosporin) and a pain-relieving gel (Burnjel) were applied to the area. Finally, 4 mg/kg of the analgesic Meloxicam (Eloxiject, Henry Schein) was injected subcutaneously to relief pain. Postsurgical care and monitoring was provided for at least 5 consecutive days.

Processing of Tissue from Electroporated Animals

Analyses of PC corticogenesis were carried out on animals at the embryonic ages of E13 (n = 5), E14 (n = 8), E15 (n = 8), E16 (n = 8), and E17 (n = 4), while PC cell linages were studied at postnatal day P21 (n = 7). The embryonic tissues were collected from CO_2 euthanized pregnant females and fixed by immersion in a 4% PFA-PBS solution for 2 days. At P21, brains were processed as described above for the analyses of thymidine analogs. All tissues were cryoprotected in a 30% sucrose-PBS solution prior to being cut in 40 µm thick consecutive sections on a Reichert Frigocut (E-2800) cryostat. P21 brains were sectioned coronally while embryonic brains were sectioned in both horizontal and coronal planes, as described in the Atlas of the Prenatal Mouse Brain (Schambra et al. 1992). Tissue sections were rehydrated in PBS and mounted with Mowiol.

Imaging and Color Postprocessing

Images were acquired using a Leica TCS-SL confocal equipped with the following laser lines: 488 (for EGFP and Alexa 488); 543 (for tdTomato and Alexa 546); and 633 (for iRFP670 and Draq5, both emitting in far-red but shown in blue). Nissl staining was imaged using an Olympus BX51 epifluorescence microscope coupled to an Olympus HKH027241 camera.

All images containing the multicolor labeling were postprocessed using Adobe Photoshop CS6 to maximize the color quality and to avoid color shifts (Cai et al. 2013), with the purpose of diminishing errors during cell quantification. The corrections applied involved blur/Gaussian filters to reduce color noise and the adjustment of pixel intensity, illumination and shading of each individual channel, and all of them were normalized to the same values for each image.

Layer Measurements, Cell Quantification, and Statistical Analysis

All quantitative measurements were done at P21 in the following regions: the anterior PC (aPC), defined as the area between the first section in which the callosum connected both brain hemispheres and the section in which the anterior commissure fascicle crossed the midline; the posterior PC (pPC), defined as the area between the section containing the most rostral part of the hippocampus and the one in which the fasciculus retroflexus is evident at the midline of the dorsal-ventral axis (Supplementary Fig. 1*D*).

The thickness of PC layers were measured on sections stained with markers characteristic of each PC layer: the LOT, only visible on aPC, was stained specifically with calretinin (CR); layer Ia was stained by the co-expression of CR and Map2; layer Ib exclusively expressed Map2; layer IIa was specifically labeled with reelin in the pPC, while in the aPC was defined by the presence of small and medium-sized pyramidal neurons observed in Nissl stained sections (O'Leary 1937); layer IIb was defined as the region of densely packed cells beneath layer IIa heavily labeled with Nissl staining; layer III was considered the area occupying the first 150 µm deep to the inner edge of Layer IIb. Measurements were made using ImageJ software on 3 representative images of both aPC and pPC (3 independent measurements per each image and finally averaged). Statistical differences were assured by applying a one-way ANOVA, followed by a Tukey posthoc test using Statistica 7.0 software.

BrdU birthdating analyses were made on 20× confocal images on both aPC and pPC, from 3 consecutive sections separated by 300 µm/each. Cell counting was performed on each PC layer as defined by calculated thickness (n = 3 for E10-E17; n = 2 for E18). The total number of cells counted was 6185. Statistical differences were assessed between layers and ages by applying a factorial ANOVA followed by an Unequal N HSD (Tukey's Honest Significant Difference for unequal sample sizes) posthoc test (Statistica 7.0). ANOVA main effects were considered to compare which layers and embryonic ages received the higher number of cells. Because we found no statistical differences between aPC and pPC data along the different layers, data from both regions were combined.

The analysis of cell progeny labeled with the multicolor technique was made on confocal stacks taken at 20× from 5 consecutive images (40 µm thick sections totaling 200 µm) on both aPC and pPC (n_{aPC} = 4; n_{pPC} = 6). Three parameters were considered for quantification: (1) layer location; (2) number of fluorophores expressed by each cell: only 1 (green, red or blue), 2 (yellow, cyan, or magenta), or all 3 together (white) (Supplementary Fig. 1*C*); and (3) if cells were neurons or glia, distinguished by morphology and validated by immunohistochemistry (Supplementary Fig. 1C; cf. Fig. 4). Data were transformed as frequency of appearance for each color label ("i"), expressed as $f_i = n_i/n_{total}$ and represented as percentage. The total number of cells counted was 7282. Statistical comparison between the expression of 1, 2, and 3 colors was performed applying a one-way ANOVA followed by a Tukey's posthoc analysis (Statistica 7.0). Differences between cell type and the aPC and pPC cortices were made by applying a factorial ANOVA followed by a Tukey's posthoc test. The phenotypic restriction of PC precursor cells was represented as heatmaps of cell frequencies adjusted to a percentile.

Results

Characterization of PC Layers

The criteria to properly delineate the distinct layers and sublayers of PC and to distinguish aPC versus pPC is challenging. CR and Map2 were previously used to identify boundaries between sublayers Ia and Ib (Sarma et al. 2011), and recently, reelin was proposed to be a specific marker for layer IIa (Diodato et al. 2016). Here, we used immunostaining against CR and Map2 to delineate PC superficial layers (LOT and layers Ia and Ib) whereas reelin and Nissl staining was used to delineate layer IIa from layer IIb in aPC and pPC respectively. Layer III was always considered the first 150 µm from the internal border of Layer IIb.

The labeling of layer Ia was consistent with the expression of both CR and Map2, while layer Ib and LOT expressed exclusively Map2 and CR, respectively (Fig. 1*A*, *B*). The LOT was not evident as a delineated structure at the light microscopy level in pPC (Fig. 1*B*). Besides LOT axon collaterals, CR also stained a small group of multipolar neurons, distributed mainly within deep layers II and III in both aPC and pPC (Fig. 1*A*, *B*), representing a subpopulation of PC interneurons previously described (Zhang et al. 2006; Garcia-Moreno et al. 2008; Gavrilovici et al. 2010). The presence of the CR^+ cells did not affect our analyses of the LOT and layer Ia. Layer Ia in aPC (146 ± 5 µm) was significantly thicker ($P < 0.01$) than layer Ia in pPC (70 ± 13 µm) and layer Ib in aPC (53 ± 4 µm), most likely due to the higher number of collaterals and axon terminals coming of the fibers from LOT (Fig. 1*E*), as suggested for rats (Schwob and Price 1984). In contrast, layer Ib in pPC (106 ± 2 µm) was significantly thicker ($P < 0.01$) than layer Ib in aPC (53 ± 4 µm) and layer Ia in pPC (70 ± 13 µm) (Fig. 1*E*).

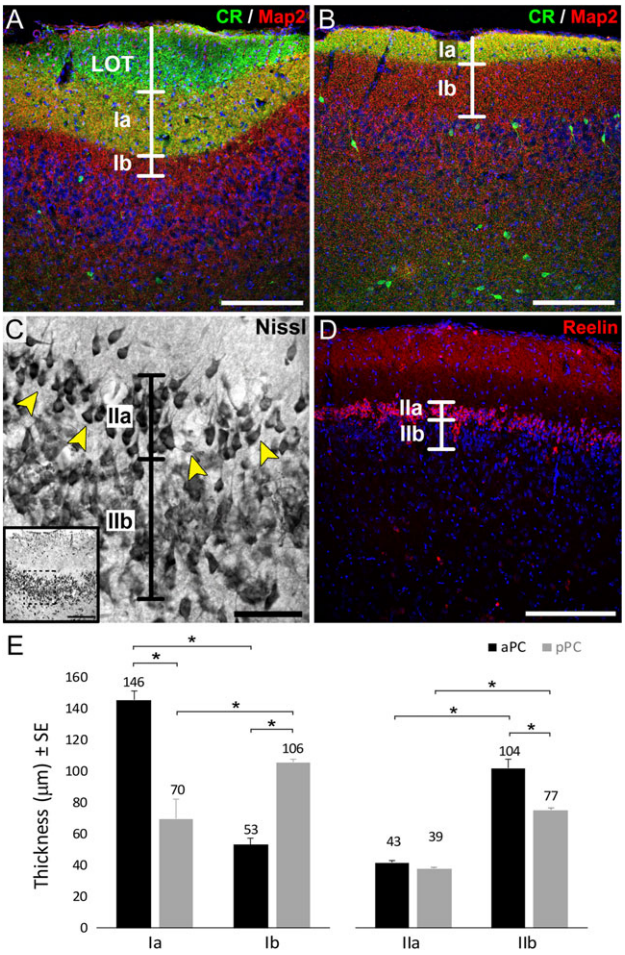

Figure 1. Characterization of PC layers. Labeling of LOT axons with the marker calretinin (CR, green), the parenchyma of layer Ia by the double expression of CR and Map2 (yellow), and layer Ib by the exclusive expression of Map2 (red) in aPC (*A*) and pPC (*B*). A subpopulation of the CR positive PC interneurons is also seen in panels *A* and *B*. (*C*) Nissl staining of aPC showing layer IIa small/medium pyramidal cells separated from large pyramidal neurons in layer IIb. The area between these layers is highlighted by the arrowheads. (*D*) Staining of pPC with reelin (red) to label layer IIa neurons. Layer IIb is defined as the remaining densely packed cells from the inner border of layer IIa. Nuclei counterstained with Draq5 (blue) in *A*, *B*, *D*. (*E*) Quantification of layers Ia, Ib, IIa, and IIb thickness measured in 3 independent samples per animal, 6 animals; *indicates $P < 0.01$. Scale bars = 200 µm in *A*, *B*, *D* and inset in *C*; 50 µm in *C*.

These data are consistent with the aPC receiving more afferent input to layer Ia from the OB compared with the pPC, which receives more associational inputs in layer Ib (Bekkers and Suzuki 2013). Considering the total thickness of the layer I (aPC: 199 ± 9 µm; pPC: 176 ± 15 µm), we did not observe a statistically significant reduction on its thickness along the anterior–posterior axis, as previously suggested (O'Leary 1937).

To establish the boundary between layers IIa and IIb in pPC we used the marker reelin, previously described as specific for layer IIa neurons (Diodato et al. 2016). We found reelin expression restricted to neurons in layer IIa of the pPC but absent from both IIa and IIb of aPC (Figs 1*D* and 2). This observation supports the notion of an anterior to posterior gradient of reelin expression in layer IIa cells (Ramos-Moreno et al. 2006), highlighting the hypothesis that molecular profiles of PC pyramidal neurons correlate with their position along this axis. Therefore, the distinction between layers IIa and IIb in aPC was made based on morphological differences. The somata of neurons in layer IIa were smaller than those found in layer IIb (Fig. 1*C*), consistent with the earliest descriptions of aPC (Calleja 1893; Ramon y Cajal 1901). The width of IIa in aPC (43 ± 1 µm) was similar to that found in reelin expressing cells of pPC (39 ± 0.9 µm) (Fig. 1*D*, *E*). Immediately deep to layer IIa, layer IIb was defined as the remaining sublaminae of densely packed cells in layer II and composed of large pyramidal neurons (Fig. 1*C*, *D*). Layer IIb was significantly thinner ($P < 0.01$) in pPC (77 ± 1 µm) than in aPC (104 ± 6 µm) and in both cases thicker than layer IIa (Fig. 1*E*).

Neurogenesis/Gliogenesis of Mouse PC

Birthdating Cell Map of PC

BrdU incorporation, which labels newly dividing cells (Wojtowicz and Kee 2006), was used to characterize neurogenesis and gliogenesis (Zhao et al. 2007) in PC, beginning at E10, when the neural tube cells are still undifferentiated, to the end of embryonic development at E18. Interestingly, we found BrdU-labeled cells in PC from the animals injected at E10, indicating that subpopulations of PC neurons originated at least 1 day earlier than in neocortex (Caviness 1982). Total cell numbers were analyzed by layers and embryonic ages in PC sections at P21. Most cells (82.3%) generated throughout all ages ended in PC deep layers, corresponding with the highly packed neuronal layers II and III (Supplementary Fig. 3A). Between embryonic ages, 80.8% of PC cells were generated in a time window ranging from E10 to E14 (Supplementary Fig. 3B), presumably with most of them migrating to the deep layers II and III (Supplementary Fig. 3A). We covered a wide range in the timeline of embryonic PC cell generation and therefore characterized if labeled cells as either neuronal or glial. The analysis of cells generated between E10 and E15 showed that the majority expressed the neuronal marker NeuN (Supplementary Fig. 4A–C) throughout the PC layers, supporting the notion that this was the window for neurogenesis. In contrast, most cells generated between E16 and E18, were negative for the neuronal marker NeuN (Supplementary Fig. 4*D*) but positive for the astroglial marker GFAP (Supplementary Fig. 4*E*–*H*), supporting the notion that PC gliogenesis occurred later in the development, as occurs in neocortex (Sauvageot and Stiles 2002). In the LOT, most of cells expressed the glial marker GFAP (Supplementary Fig. 4*F*–*H*), suggesting these cells likely belonged to glial subpopulations. There was no evidence of NeuN staining within the LOT.

Representative images of BrdU staining between layers and ages of aPC and pPC are shown in Figure 2*A* and *B*. In contrast to the early descriptions in rats (Bayer 1986), no differences were observed in the generation of cells in the aPC relative to the pPC, either between layers nor the distinct embryonic ages (Supplementary Fig. 5), indicating an absence of a posterior–anterior neurogenic gradient in PC. Because there was no evidence of a gradient in our studies, data from the aPC and pPC were combined for further analyses (Fig. 2*C*). Despite the absence of a longitudinal gradient, we observed a deep to superficial neurogenic gradient between PC layers III and II: most layer III cells were generated at E10-11 (Fig. 2*C*) while layer II cells emerged predominately between E11-14 (Fig. 2*C*), supporting the idea of an "inside-out" gradient of neurogenesis as occurs in neocortex (Rakic 2007).

Cells within the LOT were generated infrequently but uniformly during embryogenesis (Fig. 2*C*). In contrast, layers Ia and Ib exhibited both an "early-phase" at E10-11 accounting for

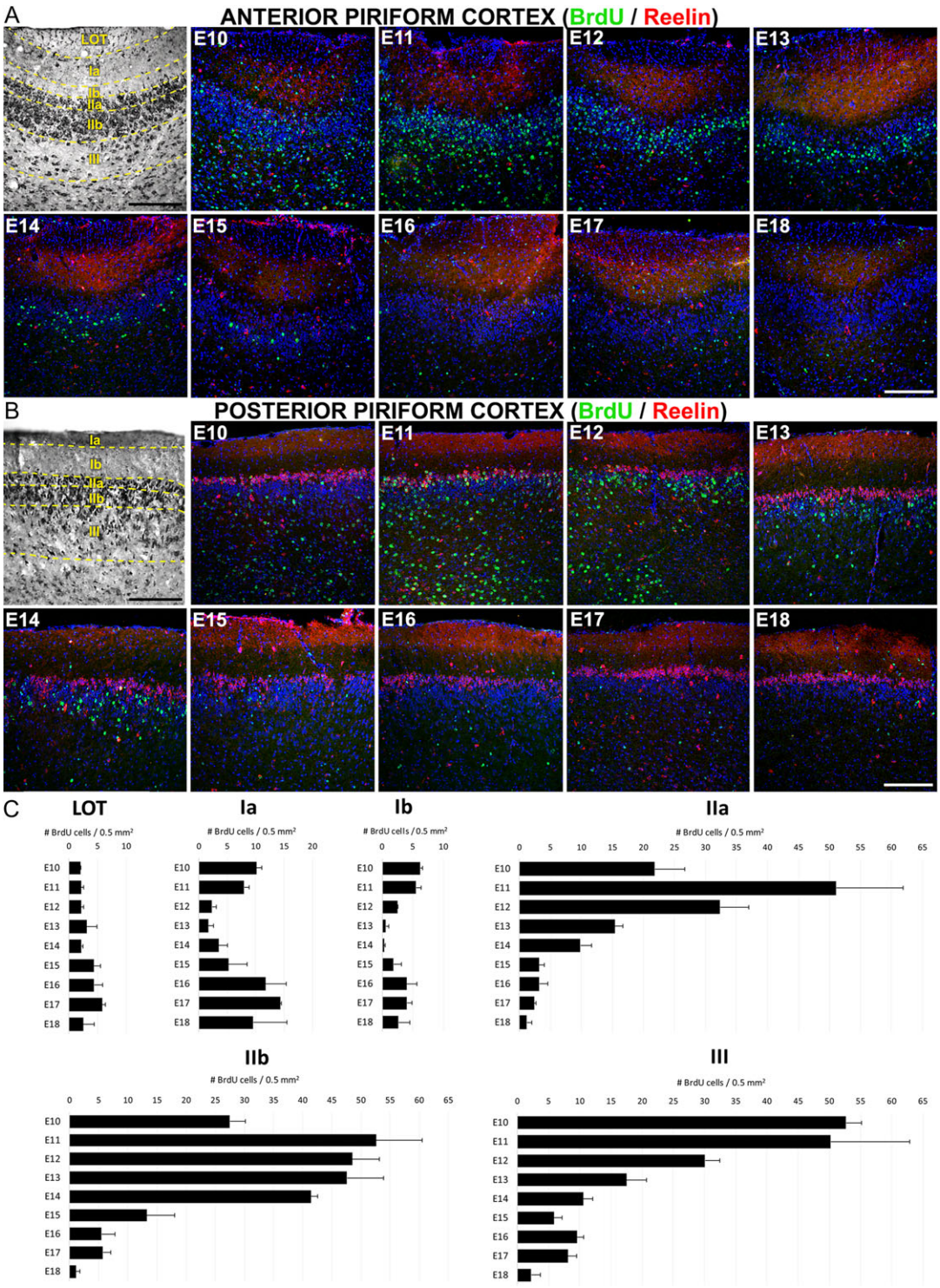

Figure 2. Mapping of PC cell birthdating analyzed by BrdU incorporation. BrdU injections were performed on pregnant mice at the gestational stages E10–E18, whereas the analysis of tissue was made at postnatal day P21. (*A* and *B*) Representative images of PC cell generation showing BrdU-labeled cells (green) generated between E10 and E18 and studied at P21 in aPC (*A*) and pPC (*B*). Brightfield images in *A* and *B* are Nissl stains to illustrate the PC layers. Reelin staining (red) is used as a guide for quantification in pPC (*B*) and it is also shown labeling layer Ia and scattered cells through PC layers in aPC (*A*). (*C*) Quantification of BrdU-labeled cells by PC layers generated between E10 and E18 and analyzed at P21. Data from aPC and pPC are not statistically different so they are shown combined. Layers Ia and Ib show 2 waves of cell generation corresponding to the injection days of E10-13 ("early-phase", corresponding to neurogenesis) and E16-18 ("late-phase", corresponding to gliogenesis). Late-phase is also seen in layer III. Nuclei counterstained with Draq5 (blue). Total number of cells counted by layers: LOT, 248; Layer Ia, 585; Layer Ib, 247; Layer IIa, 1261; Layer IIb, 2175; Layer III, 1669. Scale bars = 200 μm.

27.8% of cells in layer Ia and 42.8% of cells in layer Ib, and a *late-phase* observed at E16-18 accounting for 60.5% of cells in layer Ia and 43.4% of cells in layer Ib (Fig. 2C). In light of our analyses discussed above on the temporally-defined labeling of cells for either NeuN or GFAP, we concluded that the *early-phase* represented predominately neurogenesis while the *late-phase* represented gliogenesis. Less than 15% of layer I cells were generated between E12-14 (11% layer Ia, 12% layer Ib). Interestingly, layer Ia cells generated at E10 in aPC stayed surrounding the internal region of LOT axons (Supplementary Fig. 4I,J and Fig. 2A) resembling the behavior of a cell population derived from the guiding LOT cells (Sato et al. 1998).

In contrast to superficial layers, more than 85% of cells were generated during the E10-14 window in the deep layers of the PC, accounting 92.9% for layer IIa, 89.6% for layer IIb and 86% for layer III (Fig. 2C). Combined with the NeuN staining (Supplementary Fig. 4), these data indicated these layers received predominately neurons between E10-14. Analyzed by layers, more than 70% of layer IIa cells were generated between E10-E12 (15% at E10; 35.7% at E11; 23.1% at E12), with the cell number at E11-12 significantly higher than all other ages ($P < 0.01$). At E13, the number of labeled layer IIa cells declined to 11.2% and from E14 to E18 the number did not exceed 10% (Fig. 2C). However, the generation of cells in layer IIb exhibited a delayed temporal profile compared with layer IIa, suggesting the existence of an intra-layer superficial to deep or "outside-in" neurogenic gradient (Fig. 2C). Thus, cells generated between E11 and E14 contributed similarly to layer IIb (21.5% at E11; 20.2% at E12; 19.5% at E13; 17.1% at E14; $P < 0.01$ when comparing cell numbers to E15-18) which accounted for a delayed generation of cells respect to layer IIa. Finally, contributions to layer III showed the earliest maturation profile with an early-phase accounting for more than 70% of cells generated between E10-12 (Fig. 2C, $P < 0.01$ compared with the other ages), and a late-phase at E16-17 probably related with glial contributions (Supplementary Fig. 4).

Collectively, these results provide a detailed map of PC development organized into waves of early and delayed gradients corresponding to the neurogenesis and gliogenesis of PC. Between these waves, we noticed that PC exhibited 2 interesting mechanisms of neuronal maturation in layers II and III: an "inside-out" mechanism between layers III and layer II (inter-layer gradient); and an "outside-in" mechanism between layers IIa and IIb (intra-layer gradient). These 2 gradients support the idea of dual mechanisms of pyramidal cell maturation, as we previously suggested (Sarma et al. 2011).

Postnatal Maturation of Cells in PC

We next injected 2 groups of mice with 2 analogs of thymidine (IdU-CldU) to study the postnatal dynamics of the PC maturation, using E11–E14 as a time window. As shown in Figure 3,

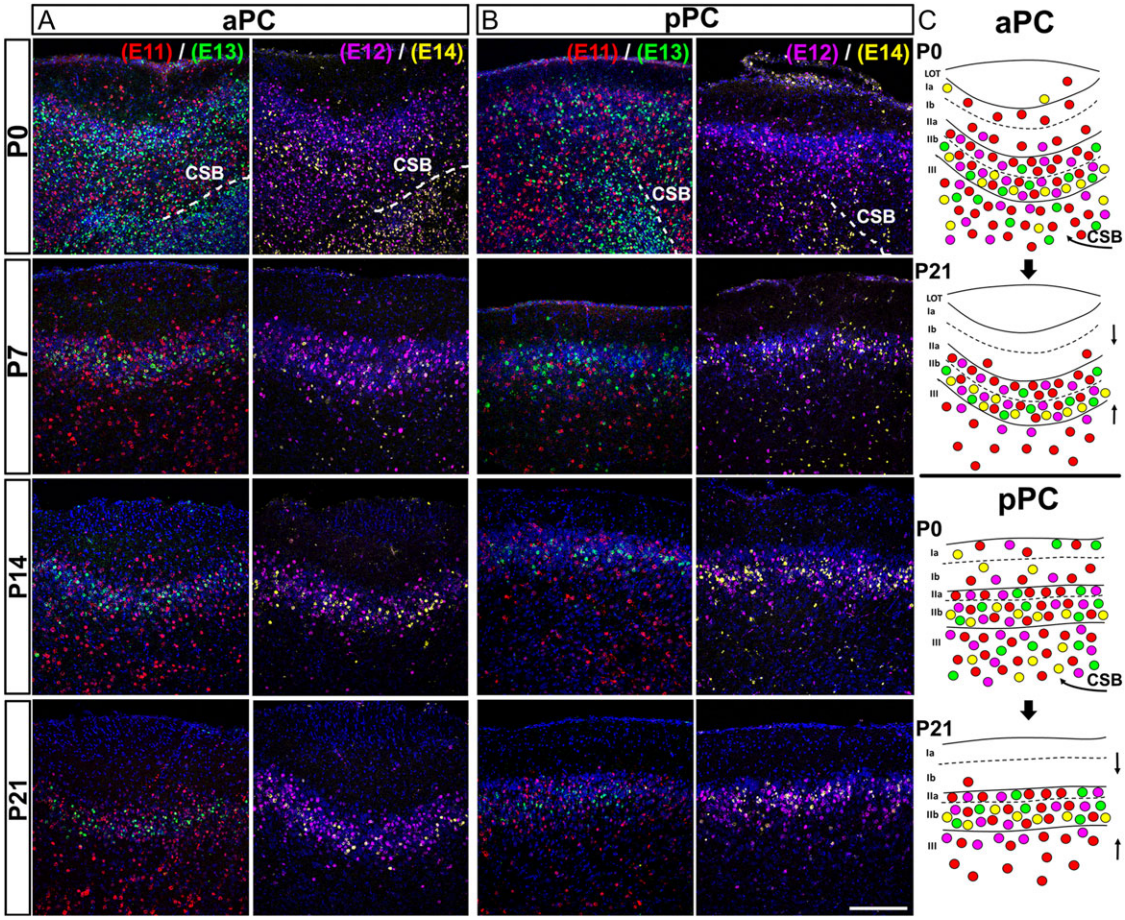

Figure 3. Postnatal maturation of anterior and posterior PC. Thymidine analogs IdU and CldU were consecutively injected in 2 set of pregnant mice at the embryonic stages E11 (red)-E13 (green), or E12 (color edited as purple)-E14 (color edited as yellow), respectively. Tissues are shown at postnatal days P0, P7, P14 and P21 and outcomes are analyzed in aPC (A) and pPC (B). Cells at P0 are widely distributed through all PC layers and cells are seen migrating from the lateral edge of the CSB (C, curved arrows) to the PC. From P7 to P21 cells are seen clustering around layer II (C, straight arrows). CSB: Cortico-Striatal Border. Scale bar = 200 μm.

there was a rearrangement of cells from the postnatal day 0 (P0) to P21 in both aPC and pPC, involving a clustering of cells around layers II and III (Fig. 3A–C). At P0 most labeled cells were distributed throughout all layers of PC, with many of them still were migrating to the PC from the ventral tip of the remaining lateral cortical stream (LCS) (Fig. 3A, B, panels at P0; Fig. 3C, curved arrows). As postnatal development progressed, cells generated at E11 (Fig. 3, red cells) and E12 (pink cells) clustered mainly around layers II and III, whereas cells generated at E13 (green cells) and 14 (yellow cells) moved from occupying the vast majority of layers II and III at P0, to be restricted into layers IIa and IIb (Fig. 3A, B). These results are consistent with the notion that the timing of neurogenesis has a significant impact on the postnatal maturation of PC (Sarma et al. 2011). Note as well that the distribution of labeled cells in layer IIa favored early born cells while those in layer IIb favored late born cells, consistent with the notion that layer II has an inverted outside-in gradient of maturation (Fig. 3C).

Influence of Cell Lineages in the Development of Mouse PC

Birthdating analysis suggested that genetic/epigenetic factors must be expressed at specific times during or after the date of cell birth influencing the migration of neuroblasts to specific layers of PC (Sarma et al. 2011). Thus, we hypothesized that the potential final phenotype and destination of progenitor cell progeny may be restricted. To address this gap in our understanding we began to interrogate whether distinct PC progenitor cell lineages determine the ultimate architecture of the PC.

A multicolor technique was used to label PC progenitor cells in the LGE, the source of PC projection neurons (Garcia-Moreno et al. 2008). As discussed in "Methods," we used the distinct code of color labeling as an approach for tracing PC cell lineages. The piggyBac transposon system is a multicolor technique that stochastically integrates different fluorescent reporter genes into the genomic DNA of cell progenitors (Garcia-Marques and Lopez-Mascaraque 2013; Martin-Lopez et al. 2013; Figueres-Onate et al. 2016). In this work, we used 3 different reporters to track cell linages during the development of PC (Supplementary Fig. 1). While the use of only 3 different reporters does impose limits on our interpretation of cell lineage, our data were sufficient to distinguish between subpopulations of cells that may allow insights into their clonal relationships. Before we implemented this approach in vivo, we validated in vitro to confirm that the 3 plasmids expressed a fluorescent signal with no overlapping emission spectra (Supplementary Fig. 2).

Characterization of Electroporated Cells in PC

We characterized the phenotype of electroporated cells in PC at P21 by immunohistochemistry (Fig. 4 and Supplementary Fig. 6). Morphologically, we found comparable cell types in both aPC and pPC distributed similarly throughout all layers of PC (Supplementary Fig. 6A,B) derived from both neuronal and astroglial lineages. We characterized the neuronal phenotypes by the expression of the neuronal marker NeuN (Fig. 4A, a, a', a"), as well as by observing the cellular morphology typically exhibited by PC neurons. Most electroporated neurons were found in layers II and III (Fig. 4). The area with labeled apical dendrites expressed the mature neuronal marker Map2 (Supplementary Fig. 6I) and occupied the extension of the CR negative area of layer I (Supplemental Fig. 6A,B). These areas coincided in size with the thickness of layer Ib thickness, as reported above (Fig. 1).

We further characterized the phenotype of electroporated neurons with a cohort of markers specifically expressed in subpopulations of neocortical neurons. Most electroporated neurons residing in layer II expressed Tbr1 (Fig. 4B, b, b', b"), a transcription factor characteristic of postmitotic projection neurons, typically pallial neurons migrating from LGE to the PC during the embryonic development. In contrast, we found that none of the electroporated cells expressed any of the typical markers of interneuron subpopulations of PC such as GAD65/67 (Fig. 4C, c, c', c"), CR (Supplementary Fig. 6A,B), GABA (Supplementary Fig. 6E,F), or parvalbumin (PV, Supplementary Fig. 6G, H) (Zhang et al. 2006), indicating we did not target regions giving rise to interneurons such as the medial (MGE) and caudal (CGE) ganglionic eminences (Lavdas et al. 1999; Wichterle et al. 1999; Xu et al. 2004). These data, together with the presence of Tbr1 in electroporated neurons, confirmed we specifically targeted PC neurons generated in the LGE. Reelin, which has previously been used to identify neurons in layer IIa (Diodato et al. 2016), was expressed by many of the electroporated cells found in layer IIa of pPC (Fig. 4D, d, d', d"). These reelin positive cells were most likely excitatory neurons of pallial origin (Carceller et al. 2016). Of interest, we identified that none of the electroporated neurons expressed either doublecortin (DCX, Supplementary Fig. 6C,D) or PSA-NCAM (Supplementary Fig. 6J), previously associated with a small subpopulation of layer II neurons (Nacher et al. 2001).

The other cell lineage observed in our samples was identified as astroglial, showing the characteristic morphology extending protoplasmic processes and expressing the astrocyte marker GFAP (Fig. 4E, e, e', e"). A subset of these cells expressed the marker S100β (Fig. 4F, f, f', f"), indicating the electroporated astrocytes belonged to different subpopulations of astroglial cells. The microglial marker IBA1 was absent in all electroporated cells indicating that microglial precursors were not targeted (Supplementary Fig. 6K, L). The presence of both neurons and glial cells confirmed that reporter genes were integrated into the genomic DNA of precursors cells (Loulier et al. 2014), targeted in the LGE, which divided through asymmetric cell division.

PC Cell Lineages are Restricted into Specific Layers During the Embryonic Development

We quantified cells expressing distinct color codes to determine if patterns in their laminar distributions would provide further insights into their clonal relationships. We validated the method by comparing the frequency of appearance (%) of the different color codes by studying cells that had incorporated 1, 2, or 3 reporter genes. As shown in Figure 5A, the probability of incorporating 3 plasmids by a single progenitor is significantly lower than the incorporation of only 1 ($P < 0.01$) or 2 ($P < 0.01$) plasmids. Thus, we can begin with the assumption that cells expressing all 3 colors have a higher probability of being part of the same lineage (Garcia-Marques and Lopez-Mascaraque 2013; Figueres-Onate et al. 2016). We recognize that interpretations of lineage relationships are ideally assessed under conditions in which only a single progenitor cell is labeled. However, with that in mind, the data reported below do show that cells expressing 3 colors are more likely to share a common fate, such as laminar position, than cells labeled with only 1 or 2 colors.

We also evaluated the frequency with which we observed all labeled neurons and glial cells in the different layers of the PC, regardless of whether they expressed 1, 2, or 3 fluorophores. Glial cells were predominantly found in layer Ia, while neurons dominated in layers IIa and IIb (Fig. 5B). The frequency of cells in the different layers was similar between the aPC and pPC (Fig. 5B).

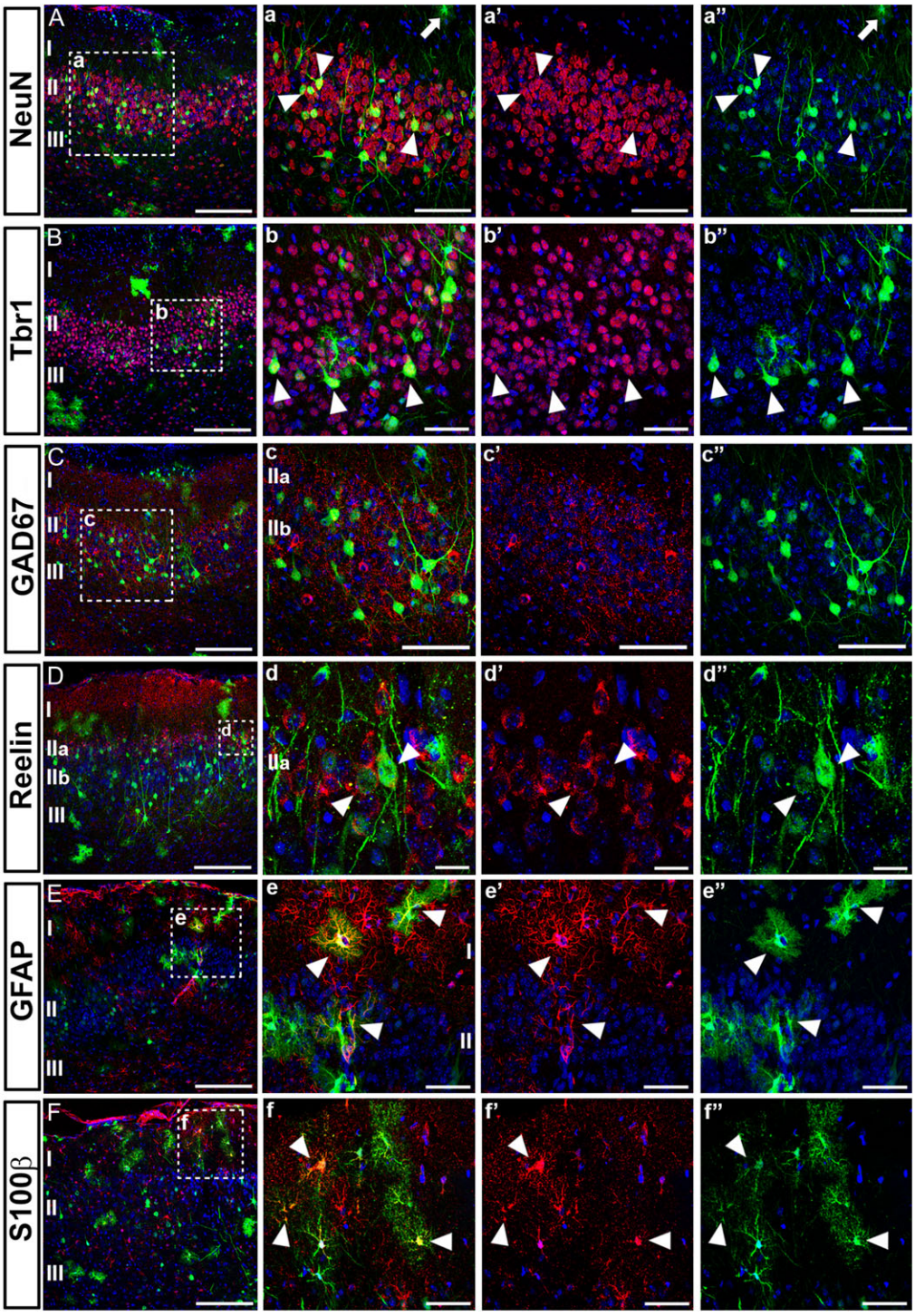

Figure 4. Molecular characterization of cells labeled by in utero electroporation. In utero electroporations were performed at E11 using a EGFP-expressing plasmid (green) and targeting the LGE. All tissues were analyzed at postnatal day P21 and subpopulations of neurons and glial cells were identified by immunohistochemistry (red). Colocalization with electroporated cells is indicated with arrowheads. Nuclei are counterstained with Draq5 (blue). (A, a, a', a") Mature neurons expressing NeuN and colocalizing with electroporated neurons were located predominately in deeper layers II and III. Cells morphologically identified as astroglia do not express NeuN (arrow). (B, b, b', b") Postmitotic projection neurons are labeled with Tbr1, which is expressed by many of EGFP cells located in layer II. (C, c, c', c") No EGFP-expressing cell express the marker for inhibitory neurons GAD65/67, indicating that electroporations were made targeting brain areas generating projection neurons. (D, d, d', d") Expression of reelin by most of the electroporated neurons located in layer IIa of pPC. (E, e, e', e") Expression of the astroglial marker GFAP by cells resembling astrocytes in the parenchyma of the upper layer I. (F, f, f', f") A subpopulation of cells morphologically resembling astrocytes expressing S100β, suggesting that LGE is the source of different subpopulation of astroglial cells. Scale bars = 200 μm in A, B, C, D, E and F; 100 μm in c, c', c"; 50 μm in a, a', a", b, b', b", e, e', e", f, f', f"; 20 μm in d, d', d".

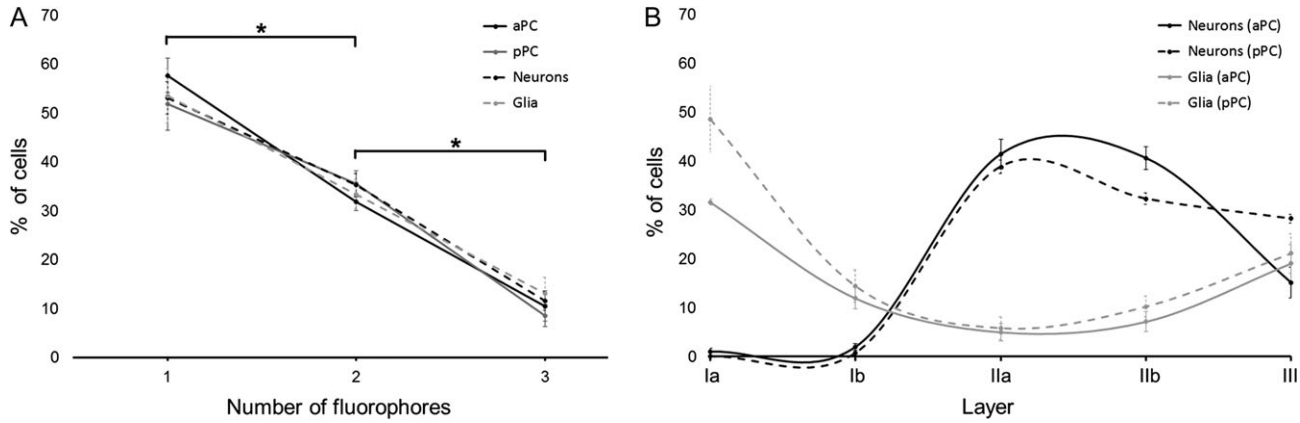

Figure 5. Multicolor technique for cell labeling based on piggyBac transposon. A mix of piggyBac transposon plasmids expressing 3 different reporter genes were electroporated in the LGE of embryos at gestational day E11. Cells that had incorporated 1, 2, or 3 plasmids were counted at postnatal day P21 in PC based on the combinations of colors expressed. The percentage of cells expressing 1, 2, or 3 colors are illustrated in (A). For both neurons and glia in both aPC and pPC approximately 54% of the labeled cells expressed 1 fluorophore, 35% expressed 2 fluorophores and only 11% expressed 3 fluorophores (ANOVA main effect for neurons: $F(2,18) = 63.2$, $P < 0.01$; glia: $F(2,18) = 24.68$, $P < 0.01$; aPC: $F(2,9) = 67.68$, $P < 0.01$; pPC: $F(2,15) = 34.36$, $P < 0.01$). In (B) the percentage of all labeled cells is shown as a function of cell type (glia versus neurons), aPC versus pPC, and PC laminae (ANOVA main effect: $F(12,80) = 40.98$; $P < 0.01$). Glial cells are predominantly seen in fibrous layer Ia in both aPC and pPC (gray lines) compared with neurons ($P < 0.01$), although a slightly higher percentage of cells was found in pPC ($P < 0.05$). In contrast, neurons were found predominantly in layers IIa and IIb in both aPC and pPC (black lines), with a significantly higher percentage than glial cells ($P < 0.01$). The percentage of labeled cells in layer III was similar for both neurons and glial cells. *indicates $P < 0.01$. Number of cells counted: 7282.

Next, we investigated whether PC cells were labeled with all 3 colors, and thus more likely to be lineage related, expressed restricted layer phenotypes. To improve quantification, we achieved a maximum color separation by editing every image acquired in both aPC (Fig. 6A) and pPC (Fig. 6C) as previously described (Cai et al. 2013). The frequency of cells that expressed 3 colors is represented as heatmaps for aPC (Fig. 6B) and pPC (Fig. 6D). For each individual, the red boxes represent the higher frequency of cell appearance. While cells expressing the 3 colors were predominantly located in a specific layer, the layer differed across animals suggesting different progenitors were targeted in each animal. Our results showed that targeted PC progenitors expressed similar phenotypes and layer distribution, suggesting those cells expressed restricted phenotypes and were thus lineage related. Considering the targeted region during the electroporation (LGE) and the molecular phenotypes expressed by these cells (Fig. 4), it was reasonable to find the distribution of neurons predominantly in layers II and III of pPC. In contrast, glial cells were found distributed along the LOT, layers Ia, Ib, and III in all individuals, suggesting that glial progenitors targeted layers throughout the PC.

Corticogenesis of PC

To further investigate how PC cells reached their final destinations, we carefully analyzed the migration routes followed by LGE precursor cells during the embryogenesis of PC (Fig. 7 and Supplementary Fig. 7). Mice electroporated at E11 were sequentially analyzed from E13 to E17 to observe the lamination dynamics of PC by neuronal cells as they populated the prospective PC. No astroglial cells were observed at these ages indicating that glial precursors had not yet reached the PC.

At E13, we observed thin cellular processes, consistent with radial glial, extending from the ventricle walls reaching the pial surface of the prospective PC in both the aPC (Fig. 7A–C) and pPC (Fig. 7D–F). As discussed previously (Misson et al. 1991; de Carlos et al. 1996), S-shaped radial processes form a scaffold that guides cells migrating ventrally through the LCS toward subpallial regions like PC. The radial processes seen in Figure 7A were likely part of these S-shaped radial cells. At this stage, most cells migrating toward the PC showed the typical leading process found in migratory cells and appeared closely apposed to the radial scaffold (Fig. 7A–F, arrowheads). At E13 laminar organization was generally not yet evident along the anterior–posterior axis although some cells had reached the PC. Some cells found in the prospective aPC surrounded the LOT (Fig. 7A). A difference between aPC and pPC was found in the maturation of neuroblasts. Most of those found in the prospective pPC have already turned their leading processes apically as presumptive apical dendrites (Fig. 7D–F, arrowhead). This maturation process followed a dorsal-ventral gradient (Fig. 7D, arrow), where more dorsal neuroblasts appeared to be organized as a distinctive layer while ventral regions were still not populated by cells. These results suggested an earlier maturation of posterior versus anterior PC.

At E14, the number of cells migrating from the LGE increased to both prospective aPC and pPC (Fig. 7G–L). At E14 pPC was forming a distinctive layer of cells (future layer II) along the whole cortex and the dorsal-ventral axis (Fig. 7J–L and Supplementary Fig. 7A). In contrast, the aPC which remained with undifferentiated layers (Fig. 7G–I and Supplementary Fig. 7A). These observations supported the idea of posterior (pPC) to anterior (aPC), and dorsal to ventral gradients of PC maturation (Supplementary Fig. 7B). Because, we showed that there were no differences in the timing of neurogenesis between aPC and pPC, this maturation gradient must be linked to differences in the migratory processes. At E14, cells belonging to the aPC were found surrounding the LOT and extending leading processes apically (Fig. 7G, H, arrowheads) similar to what occurred in pPC at E13 (Fig. 7D, E). In contrast, the pPC showed a clearly distinctive future layer II where neurons extended apical processes that frequently divided in 2 branches whose ends were lying beneath the pial surface (Fig. 7J–L and Supplementary Fig. 7A).

The 24-h delay in maturation dynamics of aPC versus pPC was still evident at E15. At E15, cells that will be part of layer II in the aPC did not yet exhibit a clear laminar pattern, although they extended apical bipolar processes towards the LOT as happened in pPC at E14 (Fig. 7M–O, arrowhead). Layer II increased in width in the pPC as cells lost the monolayer architecture and

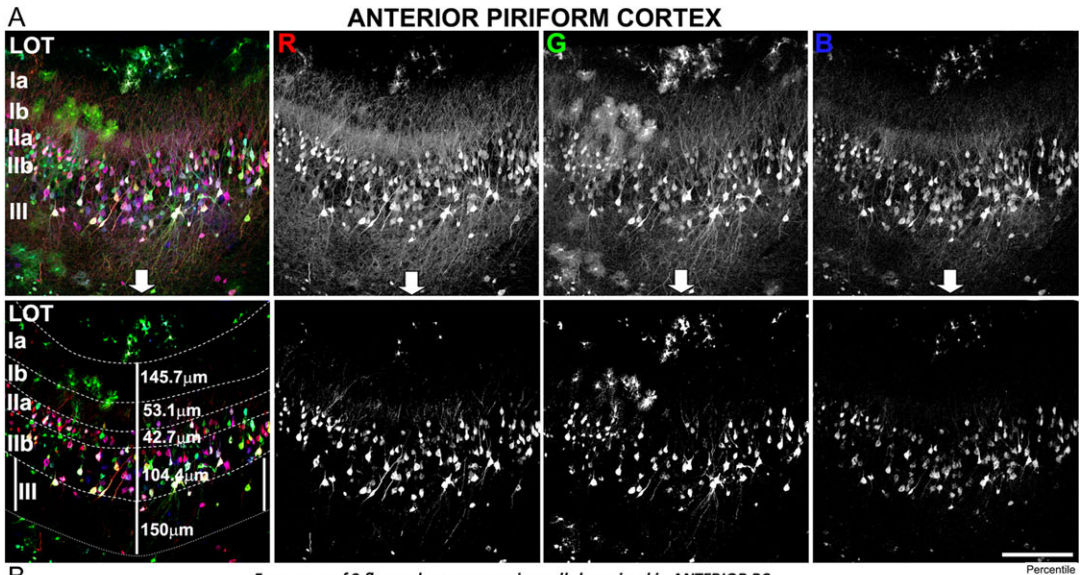

B

Frequency of 3 fluorophores-expressing cells by animal in ANTERIOR PC

Animal	Neurons							Glia						
	LOT	Ia	Ib	IIa	IIb	III	Predominant layer	LOT	Ia	Ib	IIa	IIb	III	Predominant layer
N 1	0.00	0.00	0.00	0.04	0.04	0.02	IIb	0.05	0.03	0.00	0.00	0.00	0.01	LOT
N 2	0.00	0.00	0.01	0.01	0.02	0.01	IIb	0.00	0.00	0.00	0.00	0.00	0.00	-
N 3	0.00	0.00	0.00	0.01	0.04	0.01	IIb	0.02	0.06	0.02	0.00	0.02	0.02	Ia
N 4	0.00	0.00	0.01	0.02	0.03	0.05	III	0.02	0.06	0.03	0.02	0.01	0.11	III

Percentile 90 50 10

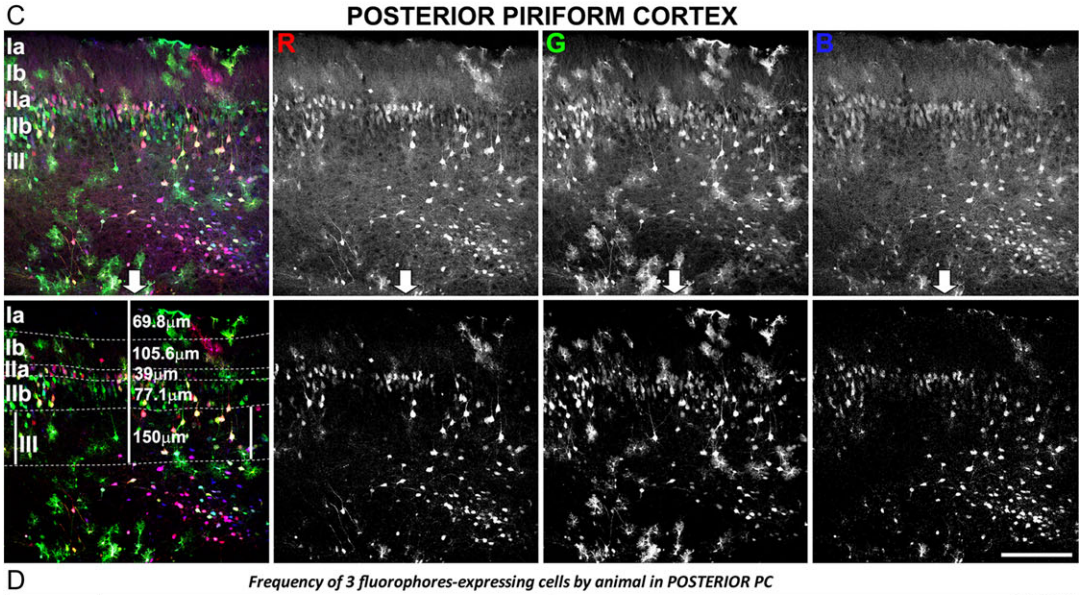

D

Frequency of 3 fluorophores-expressing cells by animal in POSTERIOR PC

Animal	Neurons							Glia						
	LOT	Ia	Ib	IIa	IIb	III	Predominant layer	LOT	Ia	Ib	IIa	IIb	III	Predominant layer
N 1		0.00	0.00	0.03	0.03	0.05	III		0.00	0.01	0.00	0.00	0.02	III
N 2		0.00	0.00	0.02	0.01	0.01	IIa		0.00	0.00	0.00	0.13	0.00	IIb
N 3		0.00	0.00	0.14	0.04	0.08	IIa		0.13	0.02	0.00	0.04	0.06	Ia
N 5		0.00	0.00	0.05	0.05	0.04	IIa & IIb		0.03	0.04	0.00	0.01	0.09	III
N 6		0.00	0.00	0.04	0.04	0.04	IIb & III		0.05	0.03	0.01	0.01	0.04	Ia
N 7		0.00	0.00	0.01	0.01	0.06	III		0.00	0.02	0.01	0.00	0.01	Ib

Percentile 90 50 10

Figure 6. Distribution of cell lineages through the PC layers. The analysis was performed at postnatal day P21 on sections of the anterior and posterior PC of animals electroporated with the multicolor technique at embryonic day E11. The interpretation of lineages was based exclusively on those cells expressing all 3 fluorophores, because they have the highest probability of belonging to the same cell lineage. Representative images of multicolored labeled cells found in aPC (*A*) and pPC (*C*) showing the distribution of cells by layers. Cells expressing 1 fluorophore can be seen in green, red, and blue; cells expressing 2 fluorophores are visualized in yellow, purple, and cyan; and cells expressing the all 3 fluorophores at the time are shown in white. Upper rows in *A* and *B* show original images taken in a confocal and the split by RGB channels. Lower rows show the image postprocessing and editing carried out on each individual channel to avoid color shifts and to facilitate quantification. (*B* and *D*): Representation of the frequency/percentage of 3-colored cell appearance by layer in aPC and pPC. Because different progenitors are targeted in each animal, data are represented individually by animal as heatmaps. Highest frequencies 3-color labeling are highlighted in red and have been interpreted as representing the highest probability of a shared lineage. Scale bars = 200 µm.

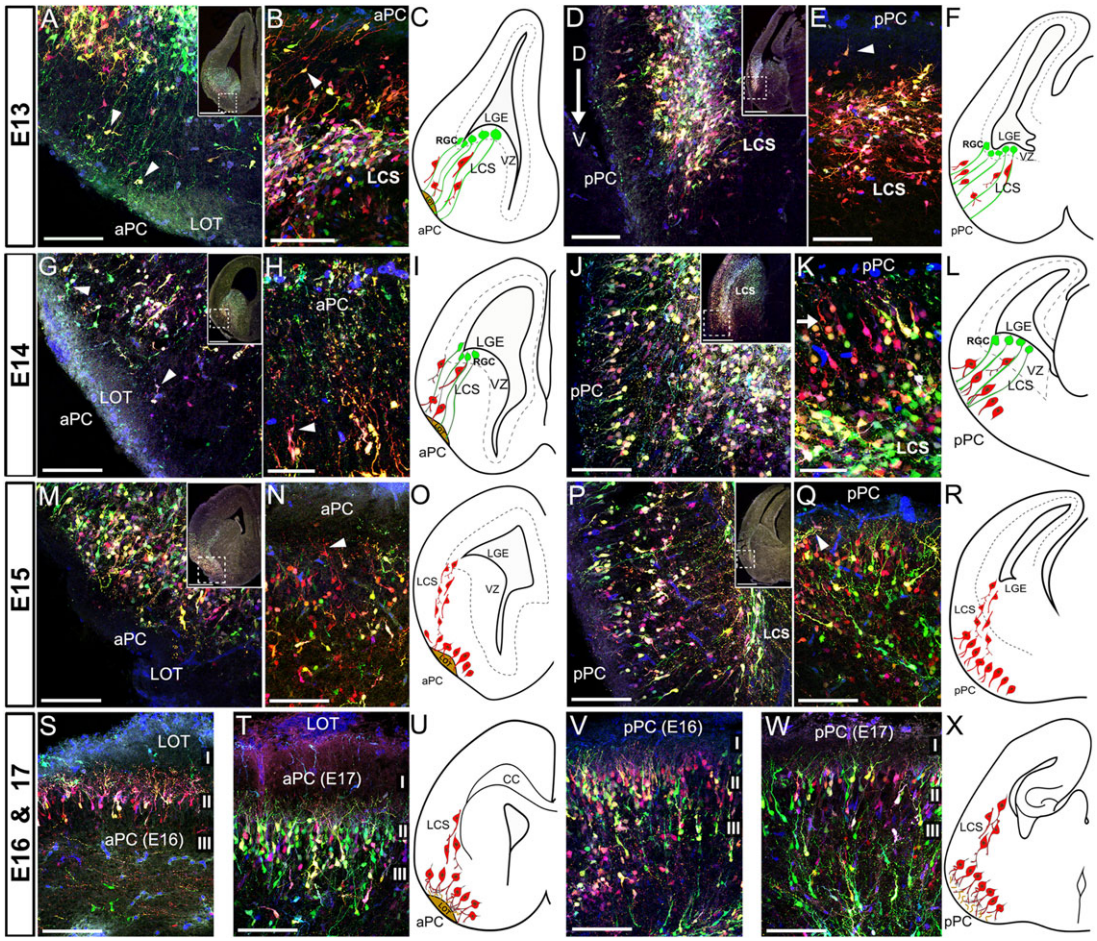

Figure 7. Dynamics of cell migration during the development of PC. The multicolor labeling technique was used to label cells in the LGE of embryos at the gestational stage of E11 by in utero electroporation. Labeled cells were sequentially studied at the embryonic ages of E13 to E17 in coronal and horizontal sections as defined by Schambra et al. (1992) in the Atlas of the Prenatal Mouse Brain. (*A*) Coronal section of an E13 embryo showing labeled cells migrating (arrowheads) from the LGE to the prospective aPC using a scaffold of cell processes that extend to the pial surface (mostly green), consistent with radial glial cells processes. No labeled cells are seen surrounding the LOT axons. (*B*) Horizontal section of the prospective aPC at E13 showing neuroblasts extending leading processes oblique to the pial surface (arrowhead) while migrating towards the PC. (*D*) Coronal section of the prospective pPC at E13 showing the arrangement of cells in a distinctive future layer II following a dorsal to ventral maturation gradient (arrow). These cells are observed detaching from the LCS toward the pPC (*E*, horizontal section; arrowheads). (*G–H*) Coronal (*G*) and horizontal (*H*) sections of the prospective aPC of an E14 embryo showing cells migrating towards the PC using the scaffold of radial glial processes (arrowheads). At this age, cell leading processes start turning to the apical surface of aPC (*G*, *H*, arrowheads). (*J–K*) Coronal (*J*) and horizontal (*K*) sections of the prospective pPC at E14, where PC neuroblasts are seen aligned as a distinctive future layer II (arrow). These cells detach from the LCS and extend bipolar branches to the apical surface and an earlier maturation of the PC is evident compared to the aPC. LCS is thickened as consequence of the increase of migrating cells (*J*, inset). (*M*, *N*) Coronal (*M*) and horizontal (*N*) sections of the aPC at E15. Neuroblast organization along the aPC is seen as a distinctive future layer II, where cells extend mostly bifurcated apical processes, as happened in pPC at E14. (*P*, *Q*) Coronal (*P*) and horizontal (*Q*) sections of the pPC at E15, where neuroblasts are observed extending multibranched apical processes and forming a multi-stratified layer II (*Q*). (*S*, *T*) Representative coronal sections of the aPC at E16 (*S*) and E17 (*T*) showing distinguishable layers I, II, and III with neuroblasts sending complex arborization to layer I. (*V*, *W*) Coronal sections of the pPC at E16 (*V*) and E17 (*W*) showing both mature PC neuroblasts forming elaborated apical processes and immature neuroblasts reaching the cortex detaching from the LCS. A posterior to anterior maturation gradient was still visible. Migratory events during the studied time-points are summarized in diagrams panels (C, E, I, L, O, R, U, X). (Abbreviations: LCS, lateral cortical stream; LGE, lateral ganglionic eminence; LOT, lateral olfactory tract). Scale bars = 500 μm in low magnification insets; 100 μm in A, B, D, E, G, J, M, N, P, Q, S, T, V, W; 50 μm in H, K.

apical dendrites extended a more elaborated/tufted arborization reaching the pial surface (Fig. 7*P–R*). Lateral dendrites became visible at this age (Fig. 7*Q*, arrowhead). At E16, neurons in layer II of aPC extended branched apical dendrites surrounding the LOT (Fig. 7*S*, *U*). Interestingly, unlike the pPC which received many migratory neuroblasts (Fig. 7*V*), the aPC received just a few cells migrating from the LCS (Fig. 7*S*, *U*). In the pPC, cells of the future layers II and III began a dense packing and the apical processes became highly branched (Fig. 7*V*, *X*). Finally, at E17 all layers in both aPC and pPC had received migratory cells from the LCS and were clearly distinguishable, resembling the architecture of the mature PC (Fig. 7*T*, *U*, *W*, *X*).

Collectively, these results suggest the maturation of the PC follows a posterior to anterior, as well as a dorsal to ventral maturation gradients, with cells arriving in the aPC ~24 h after cells reached the pPC. This difference in timing most likely reflects variation in the migration of cells but not in the timing of neurogenesis.

Discussion

Here, with an interest in understanding better the lamination of PC, we carried out a comprehensive analysis of neurogenesis and gliogenesis in PC and the influence of possible clonal

relationships among subpopulations of PC neurons and glial cells. Our data demonstrate: (1) posterior to anterior and dorsal to ventral maturation gradients in the layer specific migration of PC neurons; (2) the absence of an anterior to posterior neurogenic gradient based on cell birthdates; and (3) laminar specificity that suggests that cells derived from a common progenitor may share a similar fate in PC.

The PC is the largest olfactory cortex in mammals, extending from the caudal part of the AON to the entorhinal cortex along the entire length of the LOT (O'Leary 1937). The PC receives primary afferent input from the OB mitral and tufted cells (Haberly and Price 1977; Schneider and Scott 1983; Nagayama et al. 2010). While the anatomy, connectivity and function of the PC has been of interest for some time (Ramon y Cajal 1901; Luskin and Price 1983; Shipley and Ennis 1996; de Castro 2009; Bekkers and Suzuki 2013; Uchida et al. 2014), less is understood of the developmental profile of PC, especially in the mouse. Recent analyses of transcription factor expression revealed similarities with expression in the neocortex, with specificity for both laminar distribution and timing of neurogenesis (Brunjes and Osterberg 2015). Of further interest, the layer specific gene expression by subpopulations of PC cells is linked to projections to different areas, suggesting a functional organization not yet fully understood (Chen et al. 2014; Diodato et al. 2016). While the representation of odor information in the PC has been controversial (Stettler and Axel 2009; Sosulski et al. 2011), recent reports suggest odor information is encoded by ensembles of cells that, while invariant, are distributed across the PC without any apparent topography or spatially-defined dimension (Bolding and Franks 2017; Roland et al. 2017).

The study of the developmental dynamics of cell generation is crucial to understanding the cellular and molecular mechanisms underlying cortical development. Here, we sought to fill gaps in our understanding of mouse PC development by using contemporary tools for studying both PC neurogenesis/gliogenesis and cell lineages. We provide, for the first time, a complete and comprehensive map of mouse PC cell generation that included a pattern of laminar organization of cells generated at different embryonic stages. We began to probe the question of whether cells that originated at the same time and reached the same layer of the PC had a clonal relationship, that is, if they belong to the same cell lineage.

PC Neurogenesis/Gliogenesis

Our results demonstrated a clear relationship between the day of cell origin and their final destinations within the PC. We made a cohort of birthdating experiments to cover a wide embryonic time window ranging from embryonic Day 10 to the end of the mouse embryonic development at E18. Our results illustrated that the development of mouse PC occurred at least one day earlier than reported in rats (Bayer 1986). We detected the first postmitotic neurons at least 1 day earlier than reported for neocortex (Angevine and Sidman 1961; Caviness 1982). The developmental dynamics studied by PC layer showed 2 different mechanisms: a dual dynamic based on 2 phases (referred as "early and late phases") observed in layers I and III; and a "one-phase" dynamic observed in LOT and layer II. The phenotypic analyses using neuronal (NeuN) and astrocytic (GFAP) markers, showed that the dual dynamics likely represented the neurogenesis and gliogenesis processes occurring in layers I and III of PC, although we could not rule out the possibility of a late neurogenesis as recently described occurring with CUX1 neurons, at least at E16 (Brunjes and Osterberg 2015). In contrast, one-phase layers were likely representing gliogenesis in the LOT and neurogenesis of layer II. Interestingly, the dual dynamic of cell generation for layers I and III was also not reported in rats (Bayer 1986), showing distinct dynamics between different rodents.

Our BrdU analysis revealed that the PC development followed a double "inside-out" and "outside-in" dynamic as we previously hypothesized (Sarma et al. 2011). The "inside-out" maturation gradient appears comparable to that occurring during neocortical development (Angevine and Sidman 1961). However, the "outside-in" pattern of the cells found in layer II of PC suggests an inverted "superficial to deep" maturation gradient in layer II that could be a characteristic feature of paleocortical structures (Brunjes and Osterberg 2015). While Bayer (1986) reported a posterior to anterior neurogenic gradient in rats, we found no evidence of differing birthdates along the longitudinal axis of the mouse PC. The reason for this discrepancy is not immediately apparent, but may include species differences as well as the use of different measures for probing the timing of neurogenesis.

Analysis of Cell Lineages

The next step to better comprehend PC developmental dynamics was to assess relationships that may link specific PC cellular phenotypes, including timing of neurogenesis and laminar destination. The analysis of cell lineages can be approached with an innovative tool based on a multicolor expression technique that gives rise to the stochastic expression of several fluorophores in progenitor cells. These progenitors in turn generate progeny with unique marks or "barcodes" that they can be tracked and distinguished from neighboring cells. Working with an adaptation of the piggyBac transposon "*StarTrack*" and "*UbC-StarTrack*" methods (Garcia-Marques and Lopez-Mascaraque 2013; Martin-Lopez et al. 2013; Figueres-Onate et al. 2016), we stochastically introduced 3 different fluorophores using in utero electroporation. We targeted cells located in the LGE, which is the origin of most projection PC neurons (Bayer et al. 1991; de Carlos et al. 1996; Garcia-Moreno et al. 2008).

The ability to distinguish subpopulations of cells increases as a function of the number of stochastically incorporated color codes, effectively the length of the barcode (Cai et al. 2013). Clearly, the combination of 3 colors has a limited power to discriminate cell clones from neuronal niches and we must be conservative in interpreting the outcome of our analyses. However, our results strongly suggested that 3-colored cells presented a highly-restricted layer phenotype consistent with a common cell lineage. In addition to the color code, we narrowed the quantification area in the posterior–anterior axis to a maximum of 200 μm, a distance below which clonally related cells cluster in the neocortex (Vasistha et al. 2015). Collectively, our results suggest that those cells expressing 3 colors in PC presented a restricted phenotype in specific layers of PC therefore had a high probability of being clonally related. This conclusion was reinforced by the analysis of neuroblast migration (Fig. 7), which showed that cells did not migrate tangentially in the posterior–anterior axis after detaching from the LCS (Supplementary Fig. 7A). This observation suggested it reasonable to conclude that those cells clustered in specific layers were derived from the same cell lineage. The restricted distribution of PC cells along the anterior–posterior axis of PC appeared consistent for both neurons and glia, in agreement with the idea of a spatial conservation between related cells (Mathis and Nicolas 2000). The discrepancies reported by other authors, showing clonally related cells migrating long distances

(Kirkwood et al. 1992) could be due to differences in the method for clonal analysis.

Experiments using 3 different fluorophores have been successfully used to discriminate clonally related cells that migrate radially in columns in chick spinal cord, in which restricted migratory routes along the posterior–anterior axis were reported (Loulier et al. 2014). However, in our hands, we did not observe a columnar resolution of cells migrating to the PC. It may be reasonable to hypothesize that the PC may not emulate the columnar organization of other regions of the nervous system like the neocortex (Rakic 2009), visual system (Hubel and Wiesel 1969) or the OB (Willhite et al. 2006) as previously suggested (Chen et al. 2014). However, given the recent reports on the organization of odor representation in PC, a columnar element may be clouded by the tangential spread of cell–cell interactions and primary afferent terminations (Bolding and Franks 2017; Roland et al. 2017). For the present, the possibility of a columnar organization in PC remains an open question.

The molecular characterization of electroporated cell populations confirmed we targeted neural precursors specifically in the LGE that underwent asymmetric cell divisions. The LGE is confirmed as the main source of projection/excitatory neurons in the PC expressing Tbr1 (Garcia-Moreno et al. 2008; Pedraza and De Carlos 2012), whereas inhibitory interneurons are generated in the MGE and CGE (Lavdas et al. 1999; Wichterle et al. 1999; Xu et al. 2004). The presence of Tbr1 and the absence of any inhibitory marker in the electroporated cells suggested that the electroporation point was precise and reliable. Surprisingly, we found many of the electroporated cells located in layer IIa of the pPC expressed the marker reelin, suggesting that LGE was the origin of the this cell population. Although reelin has previously been used to label neurons in layer II of PC (Alcantara et al. 1998; Carceller et al. 2016; Diodato et al. 2016), specifically in the pPC (Ramos-Moreno et al. 2006), its function in these neurons is unknown. However, it is tempting to speculate that reelin could be involved in modulating the plasticity of layer Ia specifically in the pPC, a region rich in the apical dendrites of layer II neurons and afferent synaptic contacts (Ramos-Moreno et al. 2006). Additionally, the absence of other PC neuronal markers in electroporated cells, such as DCX, CR or PV (Nacher et al. 2001; Zhang et al. 2006) strongly suggested that these cells originated in brain regions other than the LGE. In contrast, the expression of GFAP by all detected glial cells, and the expression of S100β in some, confirmed that we targeted precursors which divided asymmetrically and gave rise to at least 2 subpopulations of astroglial cells: one $GFAP^+/S100\beta-$ and another being $GFAP^+/S100\beta^+$.

Our data demonstrated a posterior to anterior gradient in the laminar maturation of PC with pPC leading aPC by approximately 24-h. Because, this gradient is not reflected in the BrdU analyses, we concluded that it most likely reflects differences in the timing of migration. At the same time, we also observed differences in the molecular profiles of cells between the aPC and the pPC, which may have been acquired later by environmental factors. Collectively, we cannot rule out the existence of other extrinsic mechanisms induced by, for example, the arrival of LOT axons to the olfactory cortices, that could interact with determinants imposed by the PC progenitors to influence posterior–anterior gradients or the maturation of PC laminae.

Conclusions

In summary, our work leads to the following: (1) we established a detailed map of the timing of PC neurogenesis and gliogenesis by layer; (2) there are 2 gradients of PC maturation in layer II pyramidal neurons: an inter-layer "inside-out" mechanism resembling the neocortex, and an intra-layer "outside-in" mechanism observed in layer II neurons; (3) the posterior to anterior axis of PC does not show evidence of a temporal neurogenic gradient; (4) we confirm an posterior to anterior axis of reelin expression by neurons in layer IIa; (5) there is a postnatal maturation of PC based on the clustering of cells around layer II; (6) PC cell lineages show phenotypic restrictions in laminar distribution; (7) PC neuroblasts generated in the LGE migrate ventrally through the LCS to reach the PC using a scaffold of S-shaped radial glia; (8) the maturation of PC, based on the migration dynamic of cells, follows a posterior to anterior and a dorsal to ventral gradients, delayed by 24 h in the aPC as compared to the pPC; (9) the presence of astroglial cells demonstrates that LGE progenitors undergo asymmetric cell divisions during the maturation of PC cell progenitors.

Supplementary Material

Supplementary data are available at *Cerebral Cortex* online.

Funding

Supported in part by National Institutes of Health DC013791, DC015438, and DC012441 to CAG

Notes

We thank Natalia Muñoz, Miguel Lepe and Austin Jaspers for technical assistance, and members of the lab for critical reading of the manuscript and ongoing discussions. *Conflict of interest*: None declared.

References

Alcantara S, Ruiz M, D'Arcangelo G, Ezan F, de Lecea L, Curran T, Sotelo C, Soriano E. 1998. Regional and cellular patterns of reelin mRNA expression in the forebrain of the developing and adult mouse. J Neurosci. 18:7779–7799.

Angevine JB Jr, Sidman RL. 1961. Autoradiographic study of cell migration during histogenesis of cerebral cortex in the mouse. Nature. 192:766–768.

Bayer SA. 1986. Neurogenesis in the rat primary olfactory cortex. Int J Dev Neurosci. 4:251–271.

Bayer SA, Altman J, Russo RJ, Dai XF, Simmons JA. 1991. Cell migration in the rat embryonic neocortex. J Comp Neurol. 307:499–516.

Bekkers JM, Suzuki N. 2013. Neurons and circuits for odor processing in the piriform cortex. Trends Neurosci. 36:429–438.

Bolding KA, Franks KM. 2017. Complementary codes for odor identity and intensity in olfactory cortex. Elife. 6.

Brunjes PC, Osterberg SK. 2015. Developmental markers expressed in neocortical layers are differentially exhibited in olfactory cortex. PLoS ONE. 10:e0138541.

Cai D, Cohen KB, Luo T, Lichtman JW, Sanes JR. 2013. Improved tools for the Brainbow toolbox. Nat Methods. 10:540–547.

Calleja C. 1893. La region olfatoria del cerebro. ed. Madrid, España: Madrid: Imprenta y Librería de Nicolás Moya. p.

Carceller H, Rovira-Esteban L, Nacher J, Castren E, Guirado R. 2016. Neurochemical Phenotype of Reelin Immunoreactive Cells in the Piriform Cortex Layer II. Front Cell Neurosci. 10:65.

Carney RS, Alfonso TB, Cohen D, Dai H, Nery S, Stoica B, Slotkin J, Bregman BS, Fishell G, Corbin JG. 2006. Cell migration

along the lateral cortical stream to the developing basal telencephalic limbic system. J Neurosci. 26:11562–11574.
Caviness VS Jr. 1982. Neocortical histogenesis in normal and reeler mice: a developmental study based upon [3H]thymidine autoradiography. Brain Res. 256:293–302.
Ceci ML, Pedraza M, de Carlos JA. 2012. The embryonic septum and ventral pallium, new sources of olfactory cortex cells. PLoS ONE. 7:e44716.
Chen CF, Zou DJ, Altomare CG, Xu L, Greer CA, Firestein SJ. 2014. Nonsensory target-dependent organization of piriform cortex. Proc Natl Acad Sci USA. 111:16931–16936.
Choy JM, Suzuki N, Shima Y, Budisantoso T, Nelson SB, Bekkers JM. 2017. Optogenetic mapping of intracortical circuits originating from semilunar cells in the piriform cortex. Cereb Cortex. 27:589–601.
Davison IG, Ehlers MD. 2011. Neural circuit mechanisms for pattern detection and feature combination in olfactory cortex. Neuron. 70:82–94.
de Carlos JA, Lopez-Mascaraque L, Valverde F. 1996. Dynamics of cell migration from the lateral ganglionic eminence in the rat. J Neurosci. 16:6146–6156.
de Castro F. 2009. Wiring olfaction: the cellular and molecular mechanisms that guide the development of synaptic connections from the nose to the cortex. Front Neurosci. 3:52.
Diodato A, Ruinart de Brimont M, Yim YS, Derian N, Perrin S, Pouch J, Klatzmann D, Garel S, Choi GB, Fleischmann A. 2016. Molecular signatures of neural connectivity in the olfactory cortex. Nat Commun. 7:12238.
Figueres-Onate M, Garcia-Marques J, Lopez-Mascaraque L. 2016. UbC-StarTrack, a clonal method to target the entire progeny of individual progenitors. Sci Rep. 6:33896.
Garcia-Marques J, Lopez-Mascaraque L. 2013. Clonal identity determines astrocyte cortical heterogeneity. Cereb Cortex. 23:1463–1472.
Garcia-Moreno F, Lopez-Mascaraque L, de Carlos JA. 2008. Early telencephalic migration topographically converging in the olfactory cortex. Cereb Cortex. 18:1239–1252.
Garcia-Moreno F, Vasistha NA, Begbie J, Molnar Z. 2014. CLoNe is a new method to target single progenitors and study their progeny in mouse and chick. Development. 141:1589–1598.
Gavrilovici C, D'Alfonso S, Poulter MO. 2010. Diverse interneuron populations have highly specific interconnectivity in the rat piriform cortex. J Comp Neurol. 518:1570–1588.
Haberly LB. 2001. Parallel-distributed processing in olfactory cortex: new insights from morphological and physiological analysis of neuronal circuitry. Chem Senses. 26: 551–576.
Haberly LB, Hansen DJ, Feig SL, Presto S. 1987. Distribution and ultrastructure of neurons in opossum piriform cortex displaying immunoreactivity to GABA and GAD and high-affinity tritiated GABA uptake. J Comp Neurol. 266:269–290.
Haberly LB, Price JL. 1977. The axonal projection patterns of the mitral and tufted cells of the olfactory bulb in the rat. Brain Res. 129:152–157.
Hubel DH, Wiesel TN. 1969. Anatomical demonstration of columns in the monkey striate cortex. Nature. 221:747–750.
Huilgol D, Tole S. 2016. Cell migration in the developing rodent olfactory system. Cell Mol Life Sci. 73:2467–2490.
Kirkwood TB, Price J, Grove EA. 1992. The dispersion of neuronal clones across the cerebral cortex. Science. 258:317–320.
Lavdas AA, Grigoriou M, Pachnis V, Parnavelas JG. 1999. The medial ganglionic eminence gives rise to a population of early neurons in the developing cerebral cortex. J Neurosci. 19:7881–7888.
Livet J, Weissman TA, Kang H, Draft RW, Lu J, Bennis RA, Sanes JR, Lichtman JW. 2007. Transgenic strategies for combinatorial expression of fluorescent proteins in the nervous system. Nature. 450:56–62.
Loulier K, Barry R, Mahou P, Le Franc Y, Supatto W, Matho KS, Ieng S, Fouquet S, Dupin E, Benosman R, et al. 2014. Multiplex cell and lineage tracking with combinatorial labels. Neuron. 81:505–520.
Luskin MB, Price JL. 1983. The topographic organization of associational fibers of the olfactory system in the rat, including centrifugal fibers to the olfactory bulb. J Comp Neurol. 216: 264–291.
Martin-Lopez E, Garcia-Marques J, Nunez-Llaves R, Lopez-Mascaraque L. 2013. Clonal astrocytic response to cortical injury. PLoS ONE. 8:e74039.
Mathis L, Nicolas JF. 2000. Clonal organization in the postnatal mouse central nervous system is prefigured in the embryonic neuroepithelium. Dev Dyn. 219:277–281.
Misson JP, Austin CP, Takahashi T, Cepko CL, Caviness VS Jr.. 1991. The alignment of migrating neural cells in relation to the murine neopallial radial glial fiber system. Cereb Cortex. 1:221–229.
Nacher J, Crespo C, McEwen BS. 2001. Doublecortin expression in the adult rat telencephalon. Eur J Neurosci. 14:629–644.
Nagayama S, Enerva A, Fletcher ML, Masurkar AV, Igarashi KM, Mori K, Chen WR. 2010. Differential axonal projection of mitral and tufted cells in the mouse main olfactory system. Front Neural Circuits. 4. doi:10.3389/fncir.2010.00120.
O'Leary JL. 1937. Structure of the primary olfactory cortex of the mouse. J Comp Neurol. 67:1–31.
Pedraza M, De Carlos JA. 2012. A further analysis of olfactory cortex development. Front Neuroanats. 6:35.
Poo C, Isaacson JS. 2009. Odor representations in olfactory cortex: "sparse" coding, global inhibition, and oscillations. Neuron. 62:850–861.
Rakic P. 2007. The radial edifice of cortical architecture: from neuronal silhouettes to genetic engineering. Brain Res Rev. 55:204–219.
Rakic P. 2009. Evolution of the neocortex: a perspective from developmental biology. Nat Rev Neurosci. 10:724–735.
Ramon y Cajal S. 1901. Estudios sobre la corteza cerebral humana IV. Estructura de la corteza cerebral olfativa del hombre y mamíferos. Trab Lab Invest Biol Univ Madrid. 1:1–140.
Ramos-Moreno T, Galazo MJ, Porrero C, Martinez-Cerdeno V, Clasca F. 2006. Extracellular matrix molecules and synaptic plasticity: immunomapping of intracellular and secreted Reelin in the adult rat brain. Eur J Neurosci. 23:401–422.
Roland B, Deneux T, Franks KM, Bathellier B, Fleischmann A. 2017. Odor identity coding by distributed ensembles of neurons in the mouse olfactory cortex. Elife. 6. doi: 10.7554/eLife.26337.
Sarma AA, Richard MB, Greer CA. 2011. Developmental dynamics of piriform cortex. Cereb Cortex. 21:1231–1245.
Sato Y, Hirata T, Ogawa M, Fujisawa H. 1998. Requirement for early-generated neurons recognized by monoclonal antibody lot1 in the formation of lateral olfactory tract. J Neurosci. 18:7800–7810.
Sauvageot CM, Stiles CD. 2002. Molecular mechanisms controlling cortical gliogenesis. Curr Opin Neurobiol. 12:244–249.
Schambra UB, Lauder JM, Silver J. 1992. Atlas of the prenatal mouse brain. 1 ed. San Diego, CA: Academic Press, Inc. p. 327.
Schneider SP, Scott JW. 1983. Orthodromic response properties of rat olfactory bulb mitral and tufted cells correlate with their projection patterns. J Neurophysiol. 50:358–378.

Schwob JE, Price JL. 1984. The development of lamination of afferent fibers to the olfactory cortex in rats, with additional observations in the adult. J Comp Neurol. 223:203–222.

Shcherbakova DM, Verkhusha VV. 2013. Near-infrared fluorescent proteins for multicolor in vivo imaging. Nat Methods. 10:751–754.

Shipley MT, Ennis M.. 1996. Functional organization of olfactory system. J Neurobiol. 30:123–176.

Sosulski DL, Bloom ML, Cutforth T, Axel R, Datta SR. 2011. Distinct representations of olfactory information in different cortical centres. Nature. 472:213–216.

Srinivasan S, Stevens CF. 2017. A quantitative description of the mouse piriform cortex. bioRxiv. 10.

Stettler DD, Axel R. 2009. Representations of odor in the piriform cortex. Neuron. 63:854–864.

Suzuki N, Bekkers JM. 2007. Inhibitory interneurons in the piriform cortex. Clin Exp Pharmacol Physiol. 34:1064–1069.

Tantirigama ML, Huang HH, Bekkers JM. 2017. Spontaneous activity in the piriform cortex extends the dynamic range of cortical odor coding. Proc Natl Acad Sci USA. 114:2407–2412.

Uchida N, Poo C, Haddad R. 2014. Coding and transformations in the olfactory system. Annu Rev Neurosci. 37:363–385.

Uva L, Saccucci S, Chikhladze M, Tassi L, Gnatkovsky V, Milesi G, Morbin M, de Curtis M. 2017. A novel focal seizure pattern generated in superficial layers of the olfactory cortex. J Neurosci. 37:3544–3554.

Vasistha NA, Garcia-Moreno F, Arora S, Cheung AF, Arnold SJ, Robertson EJ, Molnar Z. 2015. Cortical and clonal contribution of Tbr2 expressing progenitors in the developing mouse brain. Cereb Cortex. 25:3290–3302.

Weber K, Thomaschewski M, Warlich M, Volz T, Cornils K, Niebuhr B, Tager M, Lutgehetmann M, Pollok JM, Stocking C, et al. 2011. RGB marking facilitates multicolor clonal cell tracking. Nat Med. 17:504–509.

Wichterle H, Garcia-Verdugo JM, Herrera DG, Alvarez-Buylla A. 1999. Young neurons from medial ganglionic eminence disperse in adult and embryonic brain. Nat Neurosci. 2: 461–466.

Willhite DC, Nguyen KT, Masurkar AV, Greer CA, Shepherd GM, Chen WR. 2006. Viral tracing identifies distributed columnar organization in the olfactory bulb. Proc Natl Acad Sci USA. 103:12592–12597.

Wojtowicz JM, Kee N. 2006. BrdU assay for neurogenesis in rodents. Nat Protoc. 1:1399–1405.

Xiong F, Obholzer ND, Noche RR, Megason SG. 2015. Multibow: digital spectral barcodes for cell tracing. PLoS ONE. 10: e0127822.

Xu Q, Cobos I, De La Cruz E, Rubenstein JL, Anderson SA. 2004. Origins of cortical interneuron subtypes. J Neurosci. 24: 2612–2622.

Yang J, Litscher G, Sun Z, Tang Q, Kishi K, Oda S, Takayanagi M, Sheng Z, Liu Y, Guo W, et al. 2017. Quantitative analysis of axon collaterals of single pyramidal cells of the anterior piriform cortex of the guinea pig. BMC Neurosci. 18:25.

Zhang C, Szabo G, Erdelyi F, Rose JD, Sun QQ. 2006. Novel interneuronal network in the mouse posterior piriform cortex. J Comp Neurol. 499:1000–1015.

Zhao S, Chai X, Frotscher M. 2007. Balance between neurogenesis and gliogenesis in the adult hippocampus: role for reelin. Dev Neurosci. 29:84–90.